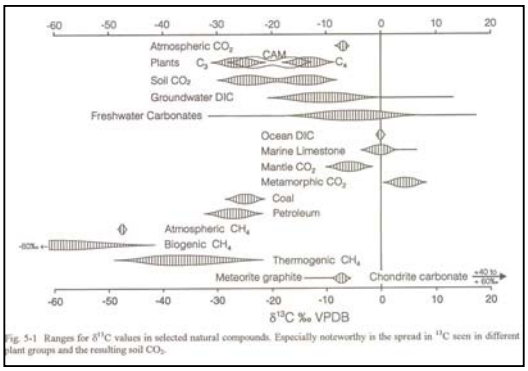

Fig. 5-1 Ranges for $\delta^{13}C$ values in selected natural compounds. Especially noteworthy is the spread in ^{13}C seen in different plant groups and the resulting soil CO_2.

Clark and Fritz, 1997.

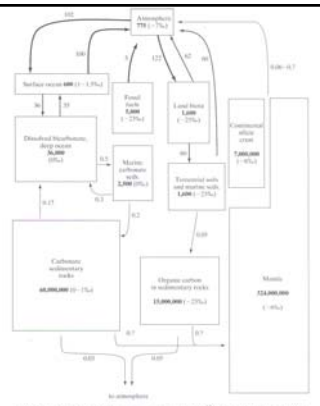

FIGURE 7.1: Carbon cycle, showing amounts, fluxes, and $\delta^{13}C$ values of different reservoirs. Abundance is shown in bold in 10^{15} g. Flux is shown in italics in 10^{15} g/yr. $\delta^{13}C$ values are in parentheses. Flux arrow thickness is proportional to relative rate.

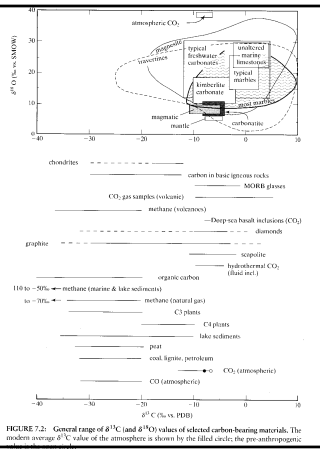

FIGURE 7.2: General range of $\delta^{13}C$ (and $\delta^{18}O$) values of selected carbon-bearing materials. The modern average $\delta^{13}C$ value of the atmosphere is shown by the filled circle; the pre-anthropogenic

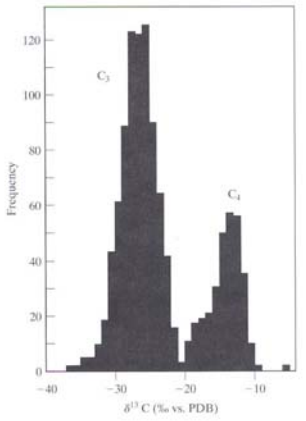

FIGURE 7.3: $\delta^{13}C$ values of C_3 and C_4 terrestrial plants. The difference of 13‰ between the two groups makes for unambiguous identification. (After Deines, 1980.)

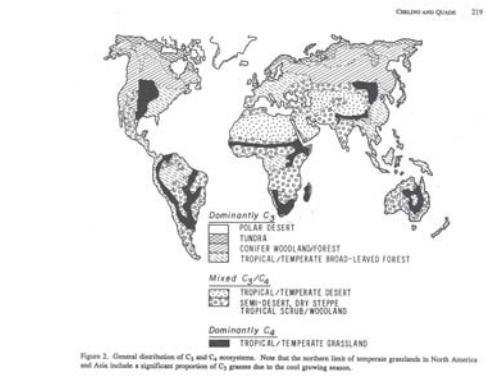

Figure 2. General distribution of C_3 and C_4 ecosystems. Note that the northern limit of temperate grasslands in North America and Asia include a significant proportion of C_3 grasses due to the cool growing season.

Cerling and Quade, 1993. Stable carbon and oxygen isotopes in soil carbonates

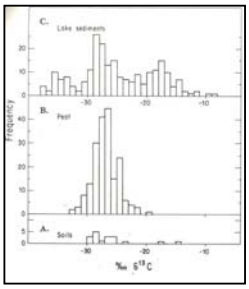

Continental organic matter CO_2 δ13C (‰ PDB).

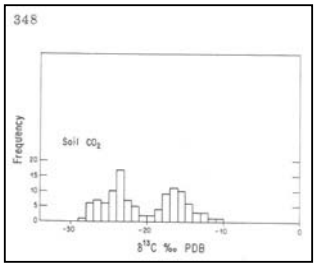

Soil CO_2 δ13C (‰ PDB).

From Deines 1980. The isotopic composition of reduced organic carbon. Fritz and Fontes, Handbook Of Environmental Isotope Geochemistry.

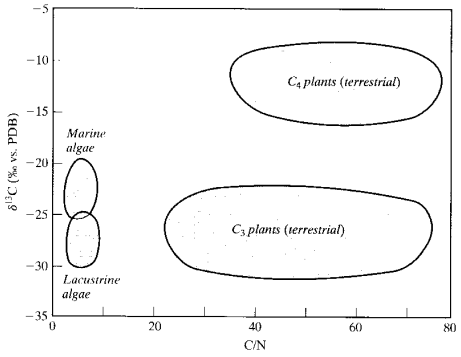

FIGURE 7.5: C/N ratios vs. $\delta^{13}C$ values of organic matter. The absence of cellulose in aquatic plants and algae leads to much lower C/N ratios than those for terrestrial plants. Minor diagenesis will not appreciably affect either C/N or isotope ratios, so that detrital material can be traced in sediments. (After Meyers, 1994.)

Carbonate solution chemistry

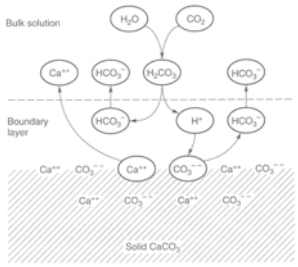

FIGURE 7–13
Steps in the solution of calcite in CO_2-bearing water. (From W. B. White, 1988, Geomorphology and Hydrology of Karst Terrains. Copyright 1988 by Oxford University Press, Inc.)

- $CaCO_3 + H_2O + CO_2 \leftrightarrow Ca_2^+ + 2HCO_3^-$

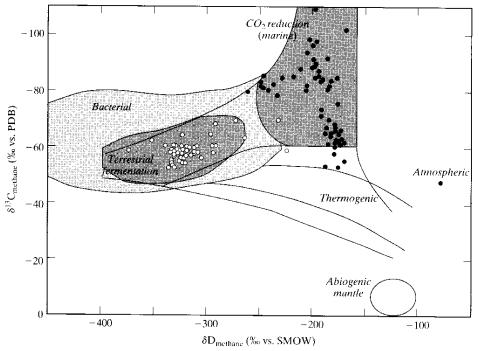

FIGURE 7.7: Combined carbon–hydrogen isotope plot of methane. With the use of combined carbon and hydrogen isotope ratios, formation from terrestrial fermentation, marine CO_2 reduction, and thermal cracking can easily be distinguished. (After Whiticar et al., 1986, and Whiticar, 1999.)

Table 27.1. Isotope Fractionation Factors of C between Carbonate Ions in Aqueous Solution, CO_2 Gas, and Solid Calcite

Compounds	$10^3 \ln \alpha$	T, °C
HCO_3^-(aq)–CO_2(g)	7.92–8.27	25
	$-0.0954T + 10.41$	7–70
CO_3^{2-}(aq)–CO_2(g)	−1.5 to +8.5	4–80
Calcite(s)–CO_2(g)	$11.98-0.12T$	10–40
Aragonite(s)–CO_2(g)	$13.88-0.13T$	10–40
Calcite(s)–HCO_3^-(aq)	1.83–2.26	25
Aragonite(s)–HCO_3^-(aq)	2.7 ± 0.2	25
Siderite(s)–HCO_3^-(aq)	−4.20 to +2.86	33–197

Source: Compiled by Chacko et al. (2001) from the literature.
Note: T = temperature in degrees Celsius.

Faure and Mensing

Anthropogenic CO2

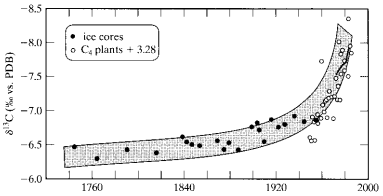

FIGURE 7.8: Variations in $\delta^{13}C$ value of atmospheric CO_2 as a function of age. Data are from direct measurements of atmospheric CO_2 (line starting in 1970), ice-core air inclusions (solid circles), and measured $\delta^{13}C$ values of C_4 maize (open circles). (After Marino and McElroy, 1991.)

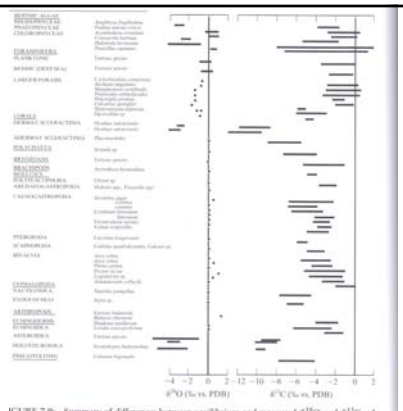

IGURE 7.9: Summary of differences between equilibrium and measured $\delta^{18}O$ and $\delta^{13}C$ values for various carbonate-secreting organisms. (Reprinted from Wefer and Berger, 1991, with permission from Elsevier.)

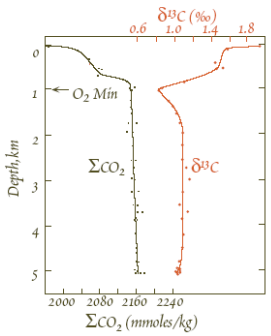

Figure 9.14. Depth profile of total dissolved inorganic carbon and $\delta^{13}C$ in the North Atlantic.

Biological Carbon Pump

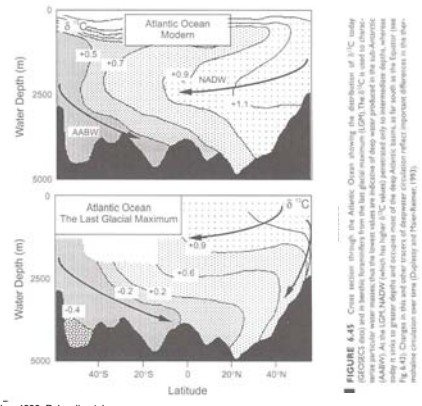

Bradley, 1999. Paleoclimatology

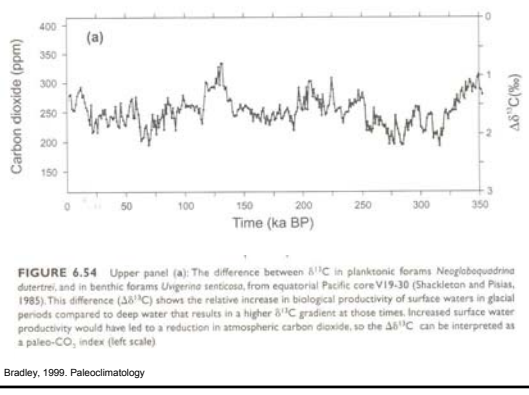

FIGURE 6.54 Upper panel (a): The difference between $\delta^{13}C$ in planktonic forams *Neogloboquadrina dutertrei*, and in benthic forams *Uvigerina senticosa*, from equatorial Pacific core V19-30 (Shackleton and Pisias, 1985). This difference ($\Delta\delta^{13}C$) shows the relative increase in biological productivity of surface waters in glacial periods compared to deep water that results in a higher $\delta^{13}C$ gradient at those times. Increased surface water productivity would have led to a reduction in atmospheric carbon dioxide, so the $\Delta\delta^{13}C$ can be interpreted as a paleo-CO_2 index (left scale)

Bradley, 1999. Paleoclimatology

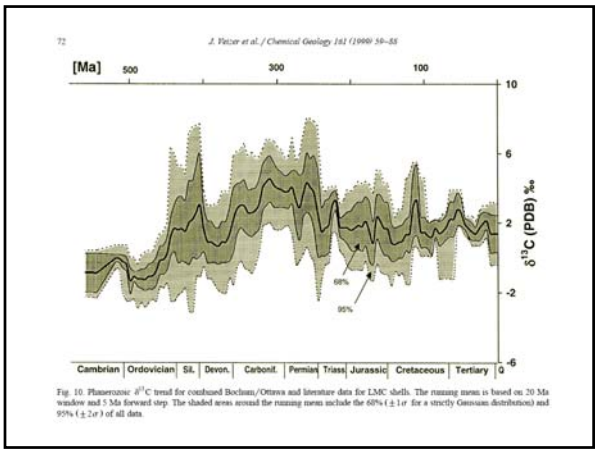

Fig. 10. Phanerozoic $\delta^{13}C$ trend for combined Bochum/Ottawa and literature data for LMC shells. The running mean is based on 20 Ma window and 5 Ma forward step. The shaded areas around the running mean include the 68% ($\pm 1\sigma$ for a strictly Gaussian distribution) and 95% ($\pm 2\sigma$) of all data.

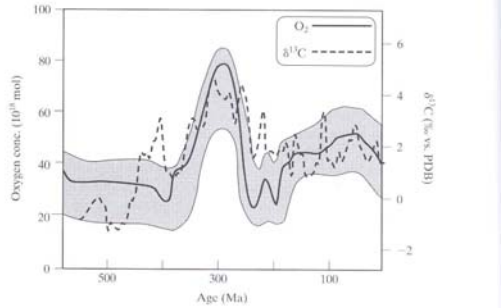

FIGURE 7.13: Correlation between the oxygen concentration of the atmosphere and the $\delta^{13}C$ value of marine carbonates. Curves from Berner and Canfield (1989) and Veizer et al. (1999).

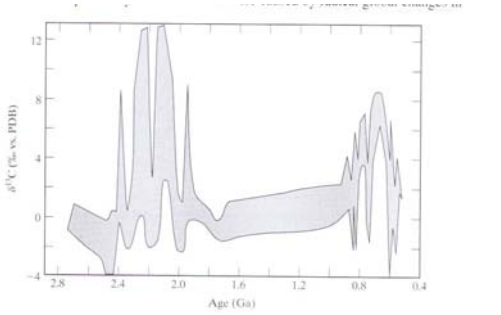

FIGURE 7.14: Carbon isotope excursions in Proterozoic carbonates. (After Des Mara

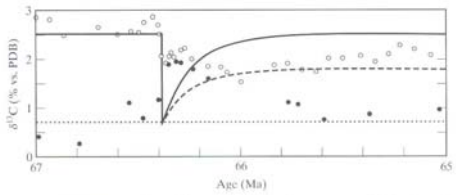

FIGURE 7.15: Variations in the $\delta^{13}C$ value of shallow-water unfilled foraminifera (P. petaloidea) and deep-water filled foraminifera (R. rotundata) across the K/T boundary. Convergence of the shallow- and deep-water foraminifera data indicate a loss of productivity and a shutdown of the biological pump. Lines show theoretical changes in carbonate $\delta^{13}C$ values across a catastrophic extinction boundary. The solid line represents the shallow-level carbonate trend with return to full recovery; the dashed line is the same, with an organic burial rate equal to 0.9 of the value before the event; the dotted line denotes the predicted deep-water carbonates. (See Zachos et al., 1989; Kump, 1991.)

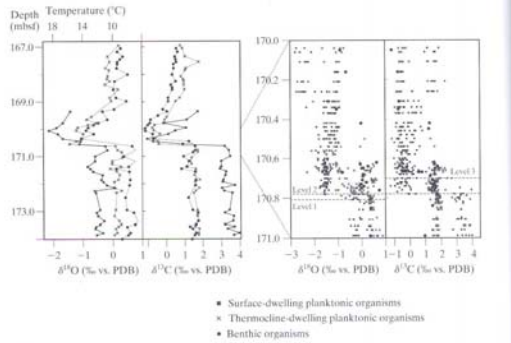

FIGURE 7.16: $\delta^{13}C$ and $\delta^{18}O$ values of benthic and planktic foraminifera across the Paleocene–Eocene boundary. Changes in $\delta^{18}O$ values indicate a warming of 5–8°C over a few thousand years. The abrupt lowering of $\delta^{13}C$ values signifies a switching off of the biological pump and the incorporation of light carbon, presumably from methane gas hydrates. (Reprinted from Jenkyns, 2003, with permission from the Royal Society of London.)

Diagenesis

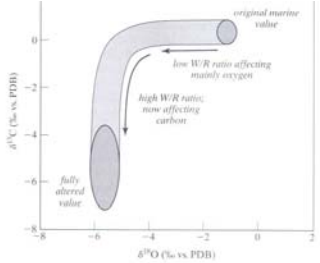

FIGURE 6.8: Illustration of changes in $\delta^{18}O$ and $\delta^{13}C$ that accompany the alteration of a marine carbonate by meteoric water. Initial dissolution and reprecipitation by interaction with pore water fluids with a small meteoric component will shift carbonates to lower $\delta^{18}O$ values but leave $\delta^{13}C$ values relatively unchanged because there is so little carbon in a water-rich fluid. Only after F/R ratios become very large, will $\delta^{13}C$ values decrease, due to exchange with light dissolved C in solution. The verticle line defined by increasing F/R interaction is sometimes called the "meteoric calcite line" (Lohmann, 1988), which defines the $\delta^{18}O$ value of meteoric water responsible for precipitation of late calcite cements.

Diagenesis

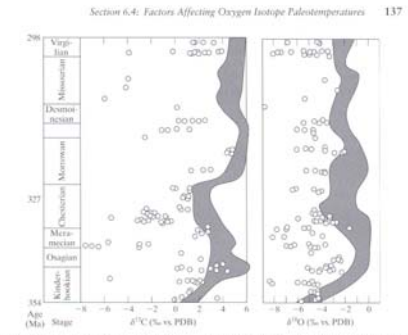

FIGURE 6.9: North American brachiopods (filled region) and coexisting cements (circles) from Carboniferous sediments. The $\delta^{18}O$ and $\delta^{13}C$ values of cements are lower than those for co-existing brachiopods, indicating diagenesis with meteoric water. Thick non-luminescent samples tend to be the least affected by diagenesis. (Modified from Mii et al., 1999.)

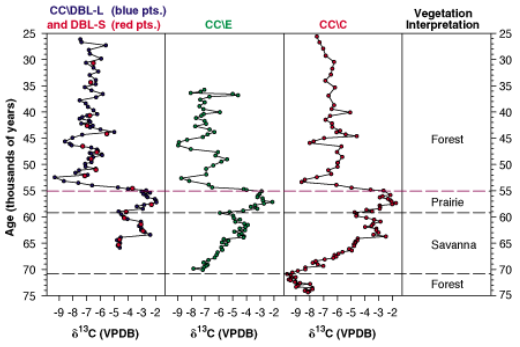

Dorale et al. 1998. *Science*, Vol 282, Issue 5395, 1871-1874

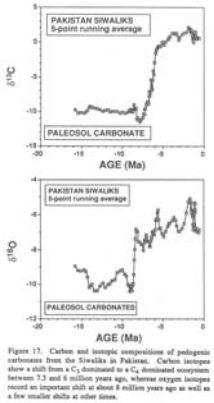

Figure 17. Carbon and isotopic compositions of pedogenic carbonates from the Siwaliks in Pakistan. Carbon isotopes show a shift from a C_3 dominated to a C_4 dominated ecosystem between 7.3 and 8 million years ago, whereas oxygen isotopes record an important shift at about 8 million years ago as well as a few smaller shifts at other times.

Cerling and Quade, 1993. Stable carbon and oxygen isotopes in soil carbonates

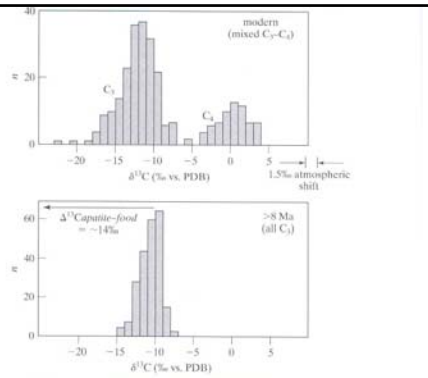

FIGURE 8.6: Carbon isotope composition of modern mammals, showing a mostly bimodal C_3–C_4 dietary preference, and of fossil mammals older than 8 Ma, which show evidence of a C_3 diet only. The $\delta^{13}C$ value of the diet is ~14 ‰ lower than that of carbonate. (After Cerling et al., 1998.)

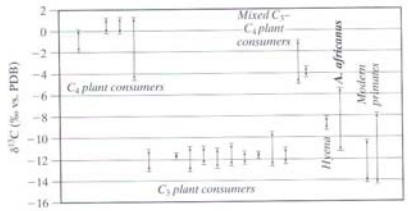

FIGURE 8.7: Carbon isotope composition of different species from the 3-Ma Makapansgat Member 3, South Africa. C_3 and C_4 plant eaters are distinct from one another. Mixed C_3–C_4 consumers and carnivores are intermediate, as is the hominid *A. africanus*. Modern primates (C_3 consumers) are also shown. (After Sponheimer and Lee-Thorp, 1999.)

Table 1 Carbon and nitrogen isotope fractionations in vertebrates

Tissue	$\Delta_{tissue\text{-}diet}$ (‰)	Subjects	Site	Source[a]
Carbon isotopes				
Apatite CO_3	+9.0–10.3	Rodents, pig	Laboratory	1–5
Apatite CO_3	+12.0–14.0	Ungulates	Field	6–8
Collagen	+0.8–3.8	Rodents, pig, quail, chicken	Laboratory	2–4, 9, 10
Collagen	+5–6	Ungulates, ostrich	Field	2, 8, 11, 12
Eggshell CO_3	+15.0	Quail, duck	Laboratory	13
Eggshell CO_3	+16.1	Ostrich	Field	12, 14,
Eggshell protein	+3.5	Quail, duck	Laboratory	13
Eggshell protein	+1.5–2.1	Ostrich	Field	12, 14
Nitrogen isotopes				
Collagen	+0.7–2.4	Rodents, pig	Laboratory	4, 15, 16
Collagen	+3.5–5.0	Mammal	Field	17
Eggshell protein	+4.2	Quail, duck	Laboratory	13
Eggshell protein	+3.0	Ostrich	Field	14

From: Koch, P.L., 1998. Ann. Rev. Earth Plan. Sci., 26: 573-613

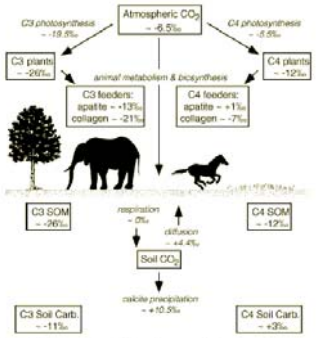

Figure 1 Carbon isotope values and fractionations among carbon-bearing materials in continental ecosystems. Fractionating processes are indicated in italics. The figure uses the pre-industrial value for atmospheric CO_2. Values for all materials, and some fractionations, will change with differences in the isotope composition and concentration of atmospheric CO_2.

From: Koch, P.L., 1998. Ann. Rev. Earth Plan. Sci., 26: 573-613

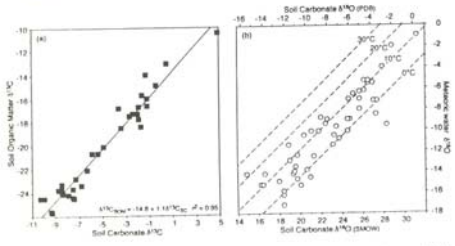

Figure 2 Relationships between (*a*) the $\delta^{13}C$ of soil organic matter and soil carbonates (PDB) and (*b*) the $\delta^{18}O$ of soil carbonate and meteoric water (SMOW) for modern soils. *Lines* represent calcite in equilibrium with meteoric water at 0° through 30°C, calculated using Equation 4. Data from Cerling & Quade (1993).

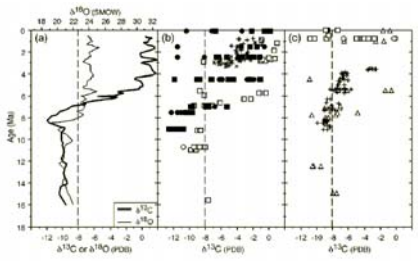

Figure 6 (*a*) $\delta^{13}C$ and $\delta^{18}O$ values of soil carbonate from Pakistan (three-point running average of data from Quade & Cerling 1995). (*b*) $\delta^{13}C$ of tooth enamel and soil carbonate in North America, including enamel from equids (*squares*) and proboscideans (*circles*) from the southwestern United States (*open symbols*) and Florida (*closed symbols*) (Wang et al 1994, MacFadden & Cerling 1996, Latorre et al 1997) and soil carbonates from Arizona (x) and New Mexico (*cross*) (Wang et al 1993, Mack et al 1994). (*c*) $\delta^{13}C$ values of tooth enamel and soil carbonate in South America, including equids (*open squares*), proboscideans (*open circles*), and toxodontids (*open triangle*) from northern Argentina and low altitude sites in Bolivia (MacFadden et al 1994, 1996, MacFadden & Shockey 1996, Latorre et al 1997) and soil carbonates in northern Argentina (*cross*) (Latorre et al 1997). $\delta^{13}C$ values greater than the *dashed lines* suggest the presence of C4 plants.

From: Koch, P.L., 1998. Ann. Rev. Earth Plan. Sci., 26: 573-613

Evolution of horses and C4 vegetation

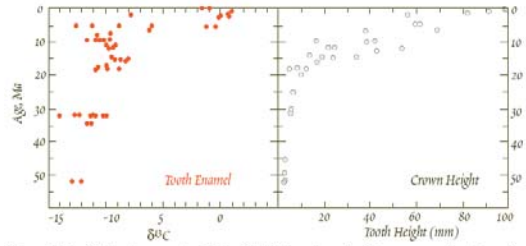

Figure 9.19. $\delta^{13}C$ and crown height in North American fossil horses as a function of age From Wang et al. (1994).